ISSN 0742-0463, Journal of Volcanology and Seismology, 2024, Vol. 18, No. 5, pp. 418–431. © Pleiades Publishing, Ltd., 2024.

Eruptive Products from the Bezymianny Volcano Eruption of April 7, 2023

V. O. Davydova[a, *], R. A. Kuznetsov[b], O. V. Dirksen[b], D. V. Melnikov[b], A. B. Ermolinskiy[a], and V. O. Yapaskurt[a]

[a] *Geological Faculty, Moscow State University, 1, Moscow, 119991 Russia*

[b] *Institute of Volcanology and Seismology FEB RAS, Piipa bulvar, 9, Petropavlovsk-Kamchatsky, 683006 Russia*

**e-mail: vestadav@gmail.com*

Received February 11, 2024; revised March 22, 2024; accepted June 27, 2024

Abstract—We have obtained the first data on the chemical composition of the eruptive materials from the explosive eruption of Bezymianny volcano on April 7, 2023. Our unique collection includes freshly sampled pumice lapilli from the eruption and juvenile blocks from pyroclastic flows. We have identified interesting patterns in both macro components and specific chalcophile elements, such as copper. The rocks we studied belong to medium-K two-pyroxene basaltic andesite (55.5–57 wt % SiO_2), with mafic enclaves characterized by a slightly more primitive composition (53.7 wt % SiO_2). According to mineral geothermometry data, the phenocrysts of basaltic andesite crystallized at temperatures in the range from 940 to 960°C, while the formation of phenocryst rims and microlites occurred at 980°C, which corresponds to conditions immediately before the eruption. The composition of volcanic glass allows us to estimate the pressure at which the magma reached the last equilibrium with crystallizing phases before eruption (0.5–0.6 kbar). Based on these findings, we have formulated hypotheses about the potential evolution of the shallow magma chamber of Bezymianny volcano during the period from 2017 to 2023.

Keywords: Bezymianny volcano, andesite, arc volcanoes

DOI: 10.1134/S0742046324700763

INTRODUCTION

Bezymianny Volcano stands in the middle of the Klyuchevskoi Volcanic Group, and is one of the more active andesitic arc volcanoes in the world. A total of 58 large explosive eruptions have occurred since the start of the recent eruption cycle (1955–1956) (Girina, 2013; Senyukov et al., 2023).

According to data reported by the Kamchatka Volcanic Eruption Response Team [KVERT, http://www.kscnet.ru/ivs/kvert/, Girina et al., 2023], the volcano's activity started to increase in late March 2023: a strong explosive eruption occurred on March 29, the eruption column rose to 6 km a.s.l. and traveled for 25 km northeastward from the volcano. Beginning April 2, debris avalanches were getting ever more frequent, and since April 5 they went down almost uninterruptedly (Girina et al., 2023). The paroxysmal eruption occurred on April 7, the eruption column rose to heights of 10–12 km a.s.l., and the ash plume traveled for more than 2000 km east-southeastward from the volcano. Pyroclastic flows as long as 6 km went down the Yuzhnaya and Vostochnaya valleys. It was estimated (Girina et al., 2023) that the volcanic explosivity index of that eruption was about 2. Members of the *Eruptivnyi* field team from the IVS FEB RAS were directly in the ashfall zone, so they have recorded how the ashfall occurred, as well as took samples of fresh material.

MATERIALS AND METHODS

The products of the paroxysmal eruption were sampled twice: during the eruption itself in April 2023, and then in August 2023.

The tephra that was produced during the eruption at some distance from the volcano had a characteristic feature (Fig. 1a, green stars), viz, a distinct bimodality of clast size, with the ash plume simultaneously dropping very fine ash and large pumice lapilli (very porous clasts of irregular shapes, mostly light grey in color) 1 to 8 cm across (Fig. 2a). To get an idea of the tephra due to the paroxysmal phases of the eruption we analyzed large pumice lapilli 3 to 5 cm across sampled on the right bank of the Sukhaya Khapitsa River on April 7, 2023 (55.938809 N, 160.767161 E) and on April 8, 2023 near Ambon Rock (see Figs. 1a, 2; 55.950000 N, 160.751650 E).

The pyroclastic flow along the Vostochnaya Valley was sampled in August 2023 (see Figs. 1a, 1b, 1c). The flow was mostly composed of fresh juvenile material.

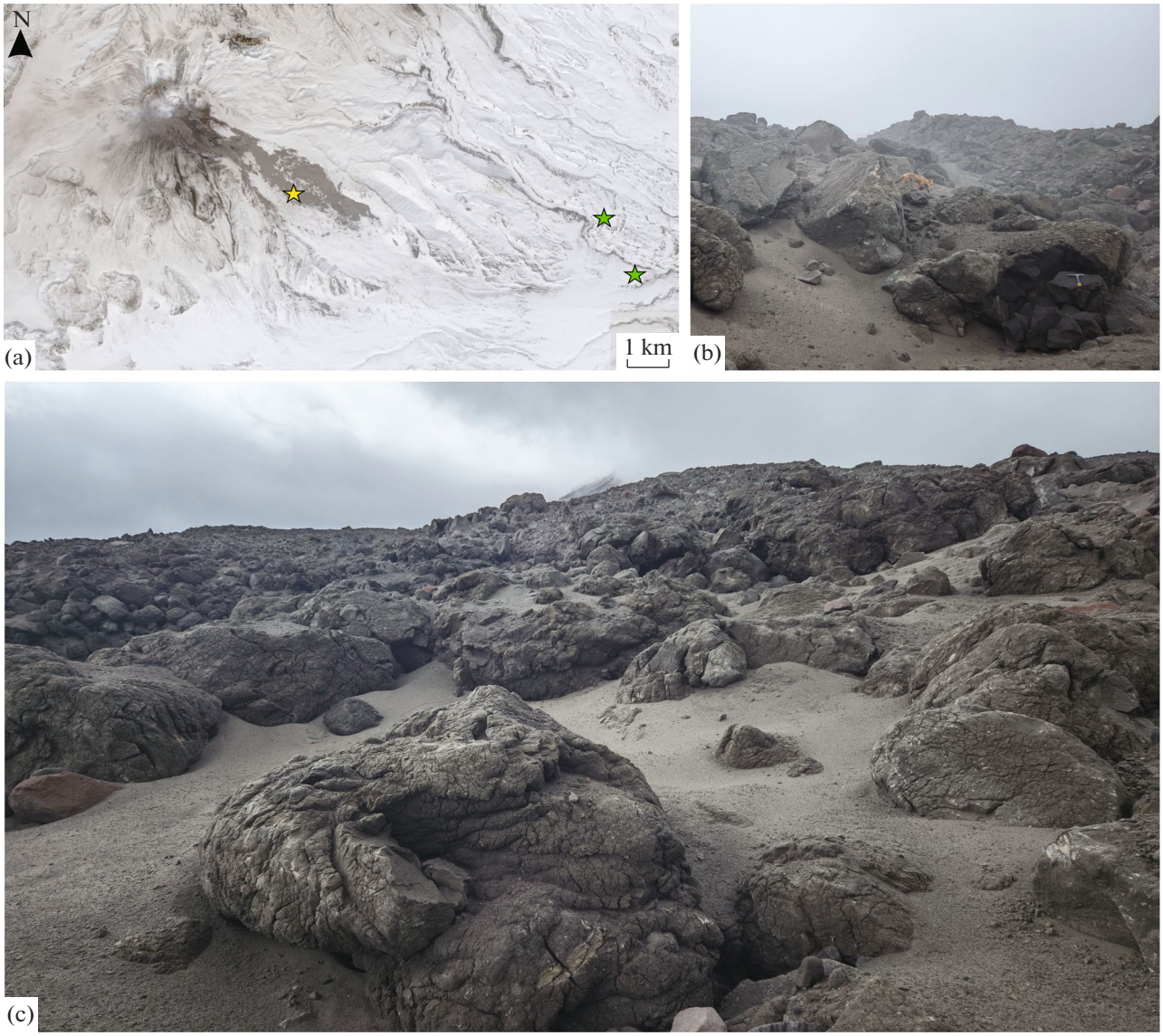

Fig. 1. The deposits discharged by the explosive Bezymianny eruption of April 7, 2023. (a) pyroclastic deposits on the Bezymianny slopes after eruption. The image was acquired from the Sentinel-2 satellite on April 29, 2023 (https://www.sentinel-hub.com/). Stars mark sampling sites in April (green) and in August (yellow) 2023; (b) inner part of a juvenile block, August 2023; (c) surface of pyroclastic flow, August 2023.

The clasts were strongly dominated by rounded blocks and bombs with traces of plastic deformation and cooling, resurgent clasts (fragments of the volcanic edifice and products of previous eruptions) being much less frequent. The largest juvenile blocks were about 5 m across, the blocks were mostly greenish-grey on the outside and dark grey, occasionally black inside. Much rarer findings are dark grey or black blocks 0.5–1 m in diameter. The rarest are angular clasts that are black, dark grey, and reddish-brown. The juvenile blocks contain mafic enclaves and xenoliths of varying genesis. For this study we analyzed samples of greenish-grey and black juvenile blocks, as well as mafic enclaves encountered.

The mineral composition was analyzed by a Jeol JSM-IT500 scanning electron microscope (SEM) equipped with an X-Max^N X-ray EDS spectrometer (Oxford Instruments) at the Department of Petrology and Volcanology, Moscow State University. Analytical conditions for the analyses were 20 kV accelerating voltage 0.7 nA and counting lifetime of 100 s. Pure synthetic oxides and natural silicates were used for calibration; the accuracy was controlled by analysis of silicate standards (Jarosewich et al., 1980). Scanning electron microscopy was also employed for backscattered electron (BSE) imaging of textures and mineral assemblages.

Fig. 2. Ashfall during the eruption of April 7, 2023. Falling pumice lapilli are clearly seen. The same can be distinguished on snow covered with fine ash (a). Lapilli on snow near Ambon Rock on the following day after the eruption (April 8, 2023, photographe d by I.A. Nuzhdaev) (b). Pumice lapilli of Bezymianny tephra immediately after sampling (photographed by V.I. Frolov) (c).

The bulk rock composition was determined at the laboratory of the analysis of mineral materials of the IGEM RAS (Moscow) by X-ray fluorescence spectroscopy (XRF) using an Axios mAX vacuum wavelength dispersive spectrometer of successive operation (PANalytical, Netherlands). The spectrometer is equipped with an X-ray tube of 4 kW power and an Rh anode, the maximum voltage on the tube is 60 kV, and the maximum anode current is 160 mA.

We determined porosity by computerized X-ray tomography using a Yamato TDM 1000H–II instrument. Porosity itself was found from tomographic results using the VGStudio Max 2.2 software. Because the lapilli under analysis had irregular shapes, we reduced the contribution of marginal effects into the result in porosity calculations by using a central cylindrical region of lapilli rather than their entire volume. Because the resolution of the tomograph is limited, our calculation was of necessity confined to pores whose linear size exceeded 0.2–0.25 mm, when the volume of the region is 2500–4100 mm^3.

Apart from determinations of porosity by computer tomography, we found volumes of samples by hydrostatic weighing method, and this enabled us to find porosity given the mass. The density of the solid component of a lapillus was assumed to be 2.67 g/cm^3 (Mueller et al., 2011).

Porosity calculations also used the analysis of panoramic BSE images using the ImageJ software and the procedure that was previously described in (Plechov et al., 2015).

A quantitative estimate of the volcanic radiative power (VRP) was determined by a method based on the analysis of multispectral nighttime observation from space using VIIRS radiometers (Visible Infrared Imaging Radiometer Suite) from Suomi NPP, NOAA-20, and NOAA-21 meteorological satellites. We used the VIIRS Nightfire (VNF) algorithm in application to a set of satellite images in visible and in nine infrared spectral ranges (Elvidge et al., 2013; Zhizhin et al., 2021). The algorithm can independently identify subpixel infrared radiators (thermal anomalies) in the short-wave (SWIR) and medium-wave infrared (MWIR) spectra, characterizing these radiators by location, size, and temperature, provided the signal exceeds the noise level in two or more infrared ranges. The algorithm can identify high-temperature (between 400 and 1600°C) sources of thermal emission, which may be lava flows or hot lava domes (Trifonov et al., 2017; Melnikov et al., 2018).

RESULTS

Bulk Composition

The samples under consideration here are consistent with basaltic andesite by their bulk rock composition (55.5–57 wt % SiO_2, Table 1). No significant differences have been detected in the bulk rock compositions of greenish-grey and black juvenile bombs and blocks of the pyroclastic flow (Fig. 3). The compositions of the bombs and the most primitive lapilli from tephra show very slight differences, with the variation among the lapilli samples being somewhat larger. The concentrations of SiO_2, MgO, and FeO vary from sample to sample, with the composition subject to the least change (sample ODV4, 55.5 wt % SiO_2, 4.4 wt % MgO, 7.9 wt % FeO) being for the least porous (from those measured) lapilli sample (68 vol % pores, Table 2), that with the greatest change (57 wt % SiO_2, 4 wt % MgO, 7.5 wt % FeO) was for the most porous, ODV2, with 76 vol % pores. The concentrations of alkalies (3.4–3.5 wt % Na_2O, ~1.1 wt % K_2O) and of other major elements vary little between samples. The sample of highest porosity (ODV2) is also somewhat depleted in Sr (290 ppm vs 310–320 ppm) and enriched in Zn and Zr (104 and 133 ppm vs 80 and 90 ppm) relative to the two other lapilli (ODV3 and ODV4), while the concentration of Rb (20 ppm) is the same in all three samples (see Table 1).

For comparison with the products of previously studied eruptions we also analyzed one mafic enclave. This has a slightly more primitive composition (53.7 wt % SiO_2, 5 wt % MgO, 8.8 wt % FeO) compared with the host rocks (basaltic andesites), which is characteristic of the Bezymianny mafic enclaves (Davydova et al., 2017).

The products of this eruption are enriched in copper compared with analogous rocks discharged by previous eruptions (1956–2019, Fig. 4a): the Bezymianny andesites and basaltic andesites typically have copper concentrations in the range 30–50 ppm (Davydova et al., 2024), while for this eruption we have 65 ppm for bombs in the pyroclastic flow and 80 ppm for lapilli. In contrast to this, the mafic enclave has a composition consistent with that for the Bezymianny inclusions that are least enriched in copper (150 ppm vs 140–330 ppm, see Fig. 4b).

Petrography

Pumice lapilli are highly porous porphyritic rocks (Fig. 5) whose phenocrysts are heavily dominated by plagioclase, as well as by orthopyroxene and clinopyroxene, and by Ti-magnetite.

The plagioclase phenocrysts do not exceed 2 mm in diameter. Most crystals possess a characteristic oscillatory zoning ($An_{47–70}$) interrupted by high-calcium zones ($An_{73–83}$) that are frequently complicated with numerous melt inclusions forming resorption zones reaching 200 μm in thickness. Less frequent are crystals with patchy-zoned plagioclase and high-Ca cores ($>An_{80}$) containing numerous melt inclusions (sieve-textured plagioclase). The compositions of microlites and rims of plagioclase phenocrysts lie in the range $An_{58–62}$.

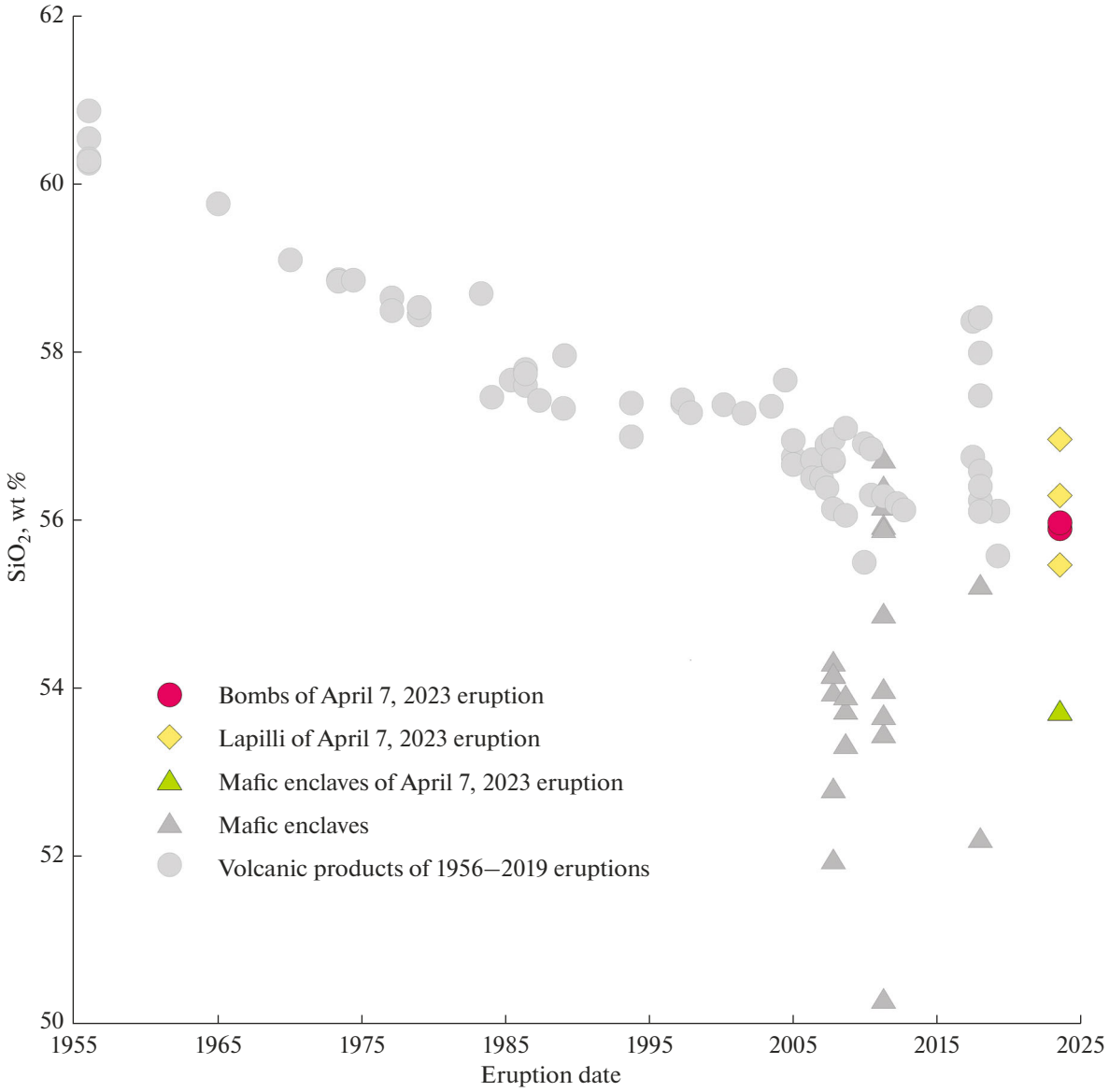

Fig. 3. The bulk rock composition of the volcanic products discharged by the April 7, 2023 eruption compared with those for other eruptions that have occurred during the current eruption cycle (the compositions are from (Turner et al., 2013; Girina et al., 2019; Davydova et al., 2022, 2024)).

Pyroxenes (up to 0.5 mm across) are characterized by simple reverse zoning, homogeneous cores (Mg# = Mg/(Mg + Fe^{2+}_{tot}): Opx—65–69, Cpx—69–72), and rims that are slightly richer in magnesium (Mg# Opx—66–76, Cpx—72–76).

Apatite is the accessory mineral, with some phenocrysts containing inclusions of ilmenite and and Fe–Cu sulfides a few μm across. It is of interest to note that our samples have not been found to contain relicts of amphibole and olivine which are encountered in products of eruptions occurring during the last few decades (Shcherbakov et al., 2011; Turner et al., 2013; Davydova et al., 2017; Davydova et al., 2022).

The groundmass is glassy, and contains rare large (20–50 μm) microlites of plagioclase and Ti-magnetite surrounded by dacitic glass (SiO_2 66.6–68.7 wt %, K_2O 2.5–2.8 wt %). The glass composition is homogeneous on average within a sample (the scatter is below 0.5 wt % SiO_2), but there was a sample containing some glass fragments of higher basicity (between 65 and 68 wt % SiO_2). The SiO_2 concentration varies by about 1 wt % among samples (see Table 2, Fig. 6),

Table 1. The bulk rock composition of samples from the volcanic products of the April 7, 2023 eruption

Sample	ODV2	ODV3	ODV4	VK2302	VK2302c	VK2302a
Type	Lapilli	Lapilli	Lapilli	Bomb	Bomb	Mafic enclave
Porosity, vol %	76	72	68			
SiO_2	56.96	56.30	55.47	55.90	55.97	53.74
TiO_2	0.79	0.80	0.83	0.80	0.81	0.97
Al_2O_3	17.97	18.14	18.03	17.98	18.20	17.94
FeO	7.46	7.57	7.89	7.64	7.68	8.83
MnO	0.15	0.16	0.17	0.16	0.16	0.18
MgO	4.09	4.23	4.44	4.31	4.32	5.06
CaO	7.86	8.18	8.44	8.25	8.15	8.86
Na_2O	3.42	3.39	3.49	3.66	3.47	3.32
K_2O	1.12	1.05	1.08	1.12	1.07	0.95
P_2O_5	0.17	0.17	0.16	0.17	0.17	0.14
LOI	1.46	0.38	0.07	0.28	0.08	0.11
Cr	47	35	51	36	38	35
V	200	179	209	174	189	216
Co	n.d.	n.d.	n.d.	23	24	25
Ni	15	14	15	18	18	21
Cu	82	81	81	65	65	152
Zn	104	78	80	74	74	79
Rb	20	20	20	22	23	19
Sr	289	319	312	322	324	319
Zr	133	91	90	99	96	83
Ba	395	427	395	415	356	341
Y	20	20	21	21	22	20
Nb	3	4	3	n.d.	n.d.	n.d.

Major elements are given as 100 wt % on dry basis, the concentrations of trace elements are in ppm; n.d. means *no data*.

without a visible correlation with the porosity of the lapilli or with their bulk rock composition.

Geothermobarometry

The temperature of magma crystallization was estimated using a two-pyroxene geothermometer (Putirka, 2008, equation 26) for a pressure of 1 kbar, which is in approximate agreement with the depth of the shallow magma chamber beneath Bezymianny (Davydova et al., 2022). A change of pressure by 1 kbar would produce a temperature change less than 5°C, which allows us to do without more detailed determinations. For these calculations we used analyses of intergrowths of orthopyroxene and clinopyroxene that have passed a test for equilibrium ($K_D(Fe–Mg)^{Cpx–Opx} = (X_{Fe}^{Cpx}/X_{Mg}^{Cpx})/(X_{Fe}^{Opx}/X_{Mg}^{Opx}) = 1.09 \pm 0.14$, Putirka et al., 2008). The crystallization temperature estimated for the central parts of the phenocrysts lie in the range 940–960°C, while the estimated crystallization temperature for the rims is 980°C.

The pressure of the last equilibrium before the eruption, roughly that at the depth of magma crystallization, was estimated by a barometer (Albarede, 1992; Putirka, 2008) based on the composition of matrix glass (silica-activity barometer). For these calculations we used estimated temperatures for pyroxene rims (980°C). The resulting values lie in the range 0.5–0.6 kbar.

Porosity

The samples for which porosity was determined have high porosity values reaching 78%. It should be noted that the values of porosity found by computerized X-ray tomography (Table 3) are appreciably

Table 2. Representative analyses of glasses when converted to 100 wt % of major oxides

No.	Porosity, vol %	SiO_2	TiO_2	Al_2O_3	FeO	MnO	MgO	CaO	Na_2O	K_2O	P_2O_5	Cl	S
ODV1		66.91	0.97	14.94	4.94	0.14	1.29	3.53	4.32	2.55	0.41	0.14	0.02
ODV1	63 (58)	66.63	1.00	14.66	5.23	0.10	1.32	3.82	4.29	2.57	0.38	0.14	b.d.l.
ODV1		67.13	1.01	14.73	4.99	0.17	1.29	3.48	4.23	2.56	0.41	0.1	b.d.l.
ODV2		67.39	0.97	14.64	4.94	0.17	1.21	3.56	4.08	2.67	0.38	0.17	0.02
ODV2	76 (68)	67.1	0.97	14.79	4.95	0.10	1.21	3.35	4.46	2.70	0.38	0.14	0.02
ODV2		67.08	0.96	14.66	4.97	0.17	1.24	3.18	4.54	2.79	0.41	0.14	b.d.l.
ODV3		65.11	0.91	15.87	5.4	0.14	1.24	4.08	4.42	2.45	0.39	0.16	0.03
ODV3	72 (61)	68.42	0.89	14.26	4.58	0.17	1.00	3.06	4.58	2.82	0.21	0.14	0.02
ODV3		68.77	0.93	14.29	4.43	0.17	1.02	2.91	4.52	2.75	0.21	0.14	0.02
ODV3		68.26	0.90	14.44	4.71	0.17	1.06	3.24	4.31	2.67	0.24	0.12	b.d.l.
ODV4		68.11	0.90	14.42	4.85	0.14	1.08	3.21	4.38	2.70	0.21	0.01	b.d.l.
ODV4		67.87	1.01	14.50	4.75	0.10	1.20	3.16	4.37	2.79	0.24	0.01	b.d.l.
ODV4	68 (42)	67.63	1.01	14.38	4.89	0.17	1.22	3.41	4.35	2.63	0.31	0.01	b.d.l.
ODV4		67.69	0.89	14.18	5.02	0.14	1.12	3.49	4.42	2.68	0.38	0.01	b.d.l.
ODV4		66.96	1.01	14.64	5.01	0.14	1.08	3.36	4.68	2.71	0.42	0.01	b.d.l.
ODV4		67.72	0.89	14.51	4.8	0.14	1.13	3.34	4.46	2.67	0.34	0.01	b.d.l.

The porosity values listed here were obtained by the method of hydrostatic weighing, those in brackets were obtained by BSE imaging; b.d.l. means *below detection threshold*.

below those determined by hydrostatic weighing in water (see Table 3). This may have been primarily due to limited resolution of the tomograph and, secondly, to the fact that the peripheral part of a sample not within the tomograph's field of vision may have greater porosity than its central part.

Remote Sensing Data

Remote sensing data (the VIIRS Nightfire algorithm) can identify with sufficient accuracy periods of an open and a closed volcanic system. The algorithm only identifies intensive thermal emission characteristic of hot extrusions or lava flows. The plot in Fig. 7

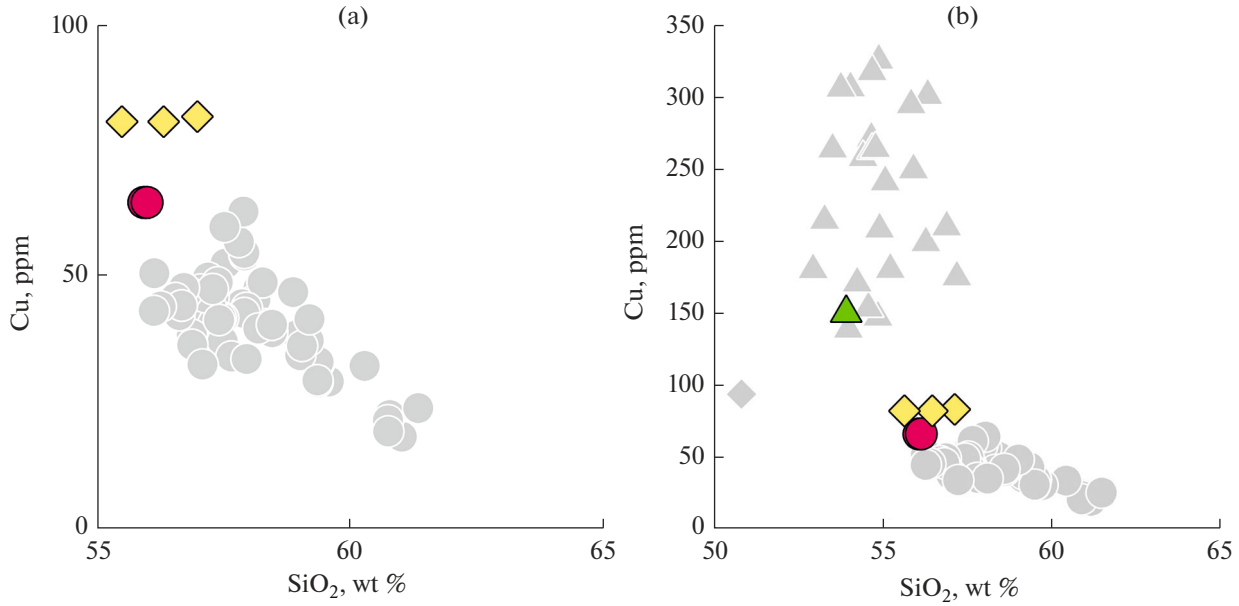

Fig. 4. Variations in the concentration of copper in the eruption products of Bezymianny. For legend see Fig. 3.

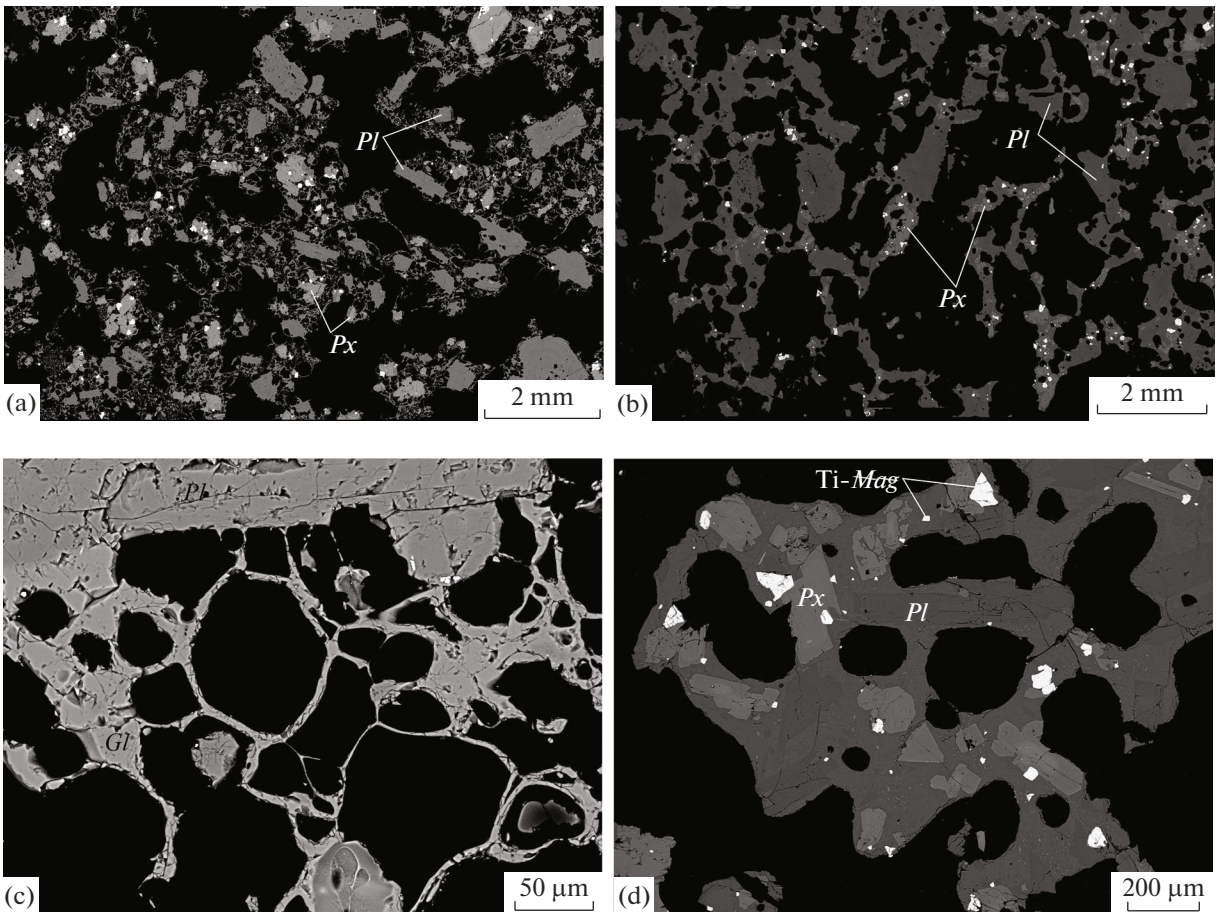

Fig. 5. The general view of eruptive products photographed in reflected electrons (a, b) and the groundmass of the samples studied here, photographed in reflected electrons (c, d). (a) ODV-2 sample (lapilli); (b) VK2302 sample (inner part of a large juvenile block from pyroclastic flow); (c) ODV-2 sample (lapilli); (d) VK2302 sample (inner part of a large juvenile block).

shows values of the power radiated by Bezymianny Volcano for the period 2012–2023. Black vertical lines mark the dates of the volcano's eruptions (the data are from the KVERT catalog, http://www.ksc-net.ru/ivs/kvert/volc?name=Bezymianny). The plot also shows the cumulative energy of volcanic thermal radiation in Joules (red curve). The periods when the volcanic system was open are marked in green.

Several periods are of interest. Following the explosive eruption of June 16, 2017, intensive thermal emission had been recorded until October 2018, which may correspond with hot extrusive blocks and the effusion of lava flows. An identical dynamics were also observed after the January 20, 2019 eruption. The system was open during the whole year, but in December 2019 there was a sudden burst of thermal emission that

Table 3. The porosity of lapilli samples found by the method of computerized X-ray tomography and hydrostatic weighing

Sample	Method of hydrostatic weighing		Computerized X-ray micro tomography		
	sample volume, mm^3	volumetric porosity	volume of cylinder for which calculation was carried out, mm^3	linear size of voxel, mm	volumetric porosity, %
OD5	20230	63	3583	0.081580	25.2
OD6	17630	72	2771	0.078152	35.4
OD7	19340	78	3250	0.073504	46.7
OD8	29300	72	4199	0.081487	38.4
OD9	24190	63	2567	0.088559	44.2

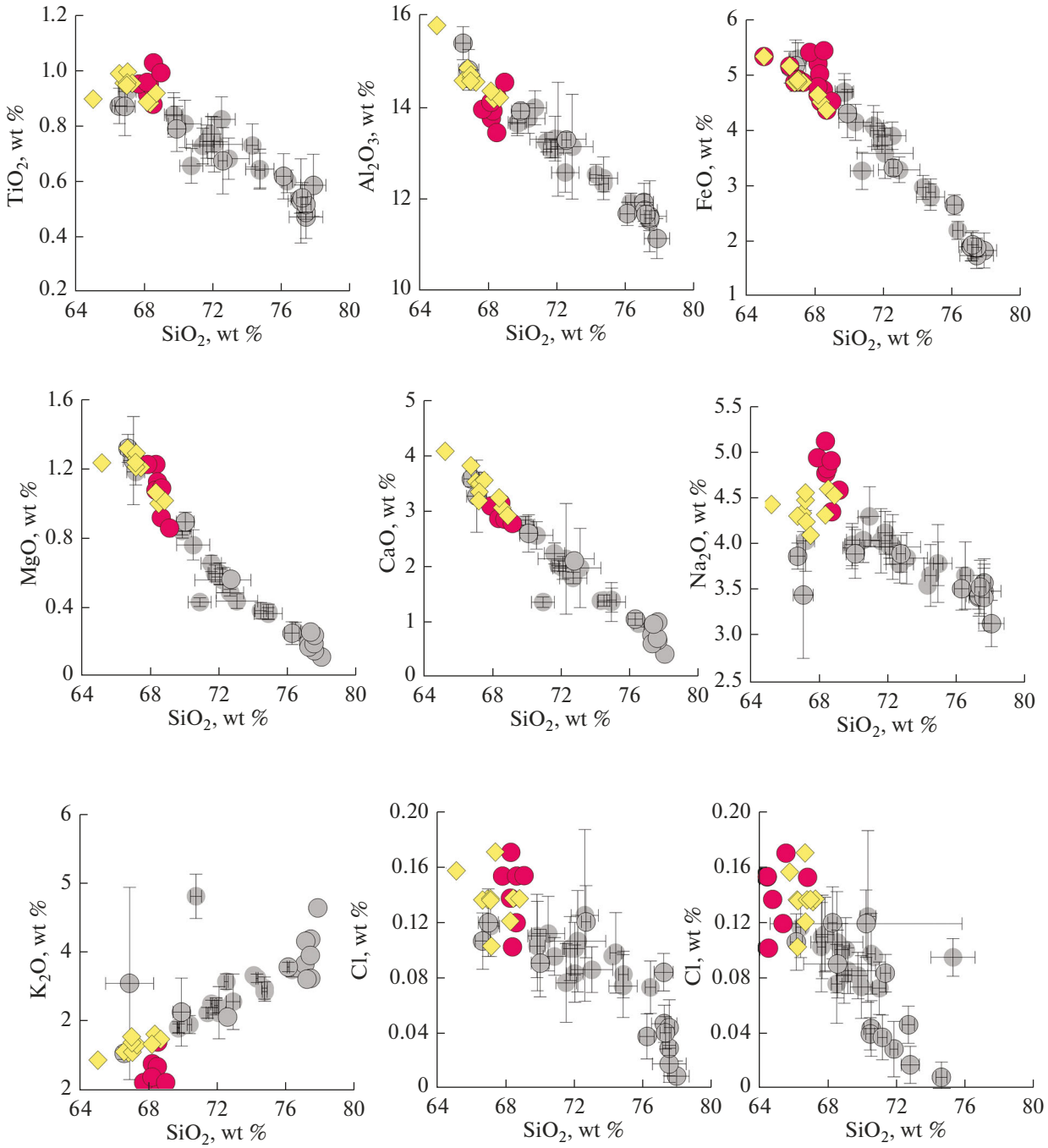

Fig. 6. The composition of volcanic glasses in the sample studied here. For legend see Fig. 3. Grey circles represent the mean compositions of glasses discharged by the 2006–2017 eruptions (Davydova et al., 2022). When there is no uncertainty bar attached, its value is less than the circle size.

was not accompanied by an explosive eruption. For the 2022–2023 period of activity we observed increasing mean values of thermal emission. Changes in the eruption activity of the volcano during that period are also indicated by seismic observations (Senyukov et al., 2023). This can probably have been due to changes in the structure of the Bezymianny magma plumbing system.

RESULTS AND DISCUSSION

The Magma Plumbing System of Bezymianny Volcano

In the course of petrologic (Davydova et al., 2017, 2018, 2022, 2024; Shcherbakov et al., 2021), geochemical (Turner et al., 2013), and geophysical (Koulakov et al., 2021; Coppola et al., 2021) studies it was shown that the present-day eruptions of Bezymianny

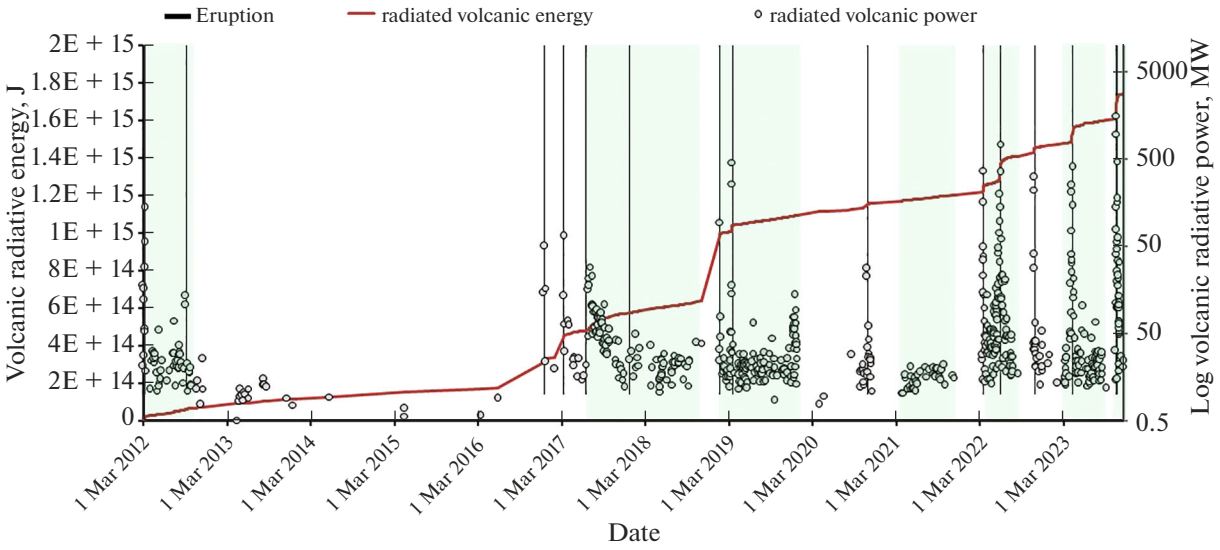

Fig. 7. A plot showing thermal emission at Bezymianny Volcano during the period 2012–2023 as determined from data of satellite VIIRS Nightfire monitoring. Red line represents cumulative radiated energy, J. The auxiliary axis shows the log volcanic radiative power, MW. Black vertical lines mark eruption dates. Green regions represent periods of open volcanic system.

are mostly initiated by the supply of magma fractionating from primitive basaltic magmas to basaltic andesitic magmas in the system of lower–middle crustal chambers (3–9 kbar) and coming into the shallow magma chamber (about 1 kbar). This ongoing supply during the recent eruption cycle (from 1955–1956 until the present) has altered the magma composition in the shallow chamber from that corresponding to hornblende dacites to two-pyroxene basaltic andesite (Turner et al., 2013; Davydova et al., 2017; Girina et al., 2020). The bulk rock composition of the feeding magmas and in magmas residing in the shallow chamber differ only slightly (by a few wt % SiO_2), but the concentration of volatiles differs considerably (at least 5 wt % H_2O in supplied magma and about 1.5 wt % in the magmas of the shallow chamber (Davydova et al., 2017; Shcherbakov et al., 2021)). The ascent of deep-stored magma to the shallow chamber and the accompanying loss of volatiles leads to several effects for both of the two mixing components.

Minerals that crystallize at deep levels (3–9 kbar, mostly the plagioclase–amphibole association) experience decompression melting as they are rising followed by subsequent recrystallization, leading to the appearance of reaction (opacite) rims in amphibole and a characteristic zoning (including patchy zoning) in plagioclase (Davydova et al., 2017). The injected deep magma is fragmented as it comes into the shallow chamber, while individual fragments (to be referred to as mafic enclaves in what follows) rapidly (a few minutes to a few hours) lose volatile components owing to diffusion over-equilibrium with the surrounding magma melt in the shallow chamber depleted in volatiles. The loss of volatiles leads to rapid crystallization of the mafic enclaves, until they have reached equilibrium with the magma of the shallow chamber (Davydova et al., 2024). When residing in the shallow chamber for a long time, some of the enclaves are destroyed, resulting in the appearance of characteristic relict crystals of plagioclase and amphibole in the magmas of the shallow chamber. It thus appears that the presence of both destroyed mafic enclaves (the presence of relict cores of plagioclase phenocrysts with patchy zoning) and of preserved mafic enclaves in the pyroclastic deposits of this eruption correspond with signs providing evidence of supply from lower levels of the magma plumbing system as pointed out in previous publications (Shcherbakov et al., 2011, Turner et al., 2013; Davydova et al., 2017, 2022).

The addition of volatile components to the magma in the shallow chamber leads to partial melting of the formed crystals and to subsequent intergrowth of rims enriched in a higher-temperature endmember and frequently complicated with resorption zones (Davydova et al., 2017, 2018]. In this way the normal (for pyroxene) or oscillatory (for plagioclase) zoning in phenocrysts that is formed during crystallization in a convecting magma chamber (Shcherbakov et al., 2021) is interrupted by melting zones that characterize episodes of new deep-stored magma portions being supplied to the shallow chamber. The eruptive products of April 7, 2023 show the same pattern, thus also providing evidence of a persisting mechanism of eruption initiation at the volcano.

The emplacement of deep-stored magma and the addition of fluid components results in an increasing pressure in the shallow chamber. When the critical value has been reached, the magma is extruded into the magma conduit to be followed by magma fragmentation and subsequent eruption. The depth at

which magma fragmentation occurs is "recorded" by the composition of volcanic glass corresponding with the composition of the last equilibrium between the melt and crystallizing microlites. Knowing that the latent heat of crystallization ensures a crystallization temperature for microlites that is slightly above that for phenocryst cores (Shcherbakov et al., 2011), as also knowing that microlites are formed during the rise of magma in the conduit, we hypothesize that the melt temperature during fragmentation would not be below that of microlite crystallization. In this way we can make a rough estimate for the pressure corresponding with the depth where magma fragmentation started before the April 7, 2023 eruption (0.5–0.6 kbar).

Eruption Products and Their Evolution Relative to Previous Eruptions

Lapilli porosity. This was estimated using three independent methods, viz, computerized X-ray tomography, hydrostatic weighing, and analysis of panoramic BSE images using the ImageJ program. The greatest porosity values were obtained by weighing samples in water (63–76 vol %), and the least using the method of computer tomography (25–46 vol %). The analysis of large-scale BSE images allows one to identify porosity variations in a sample, which can occasionally reach 20 vol %; overall, the estimates lie in the range 40–70 vol %. As well, BSE imaging enables estimation of pore size, some of the pores being considerably below the smallest size necessary for correct use of computerized X-ray tomography. Bearing in mind the procedure used to prepare polished sections (for porous samples one commonly chooses the strongest part, which is accordingly the least porous), one arrives at the obvious conclusion that porosity measurements of such samples by hydrostatic weighing must yield the most correct results (63–76 vol % for lapilli discharged by the April 7, 2023 eruption).

Estimates of porosity using the method of BSE imaging overlap with those for some of the volcanic products discharged by the April 7, 2023 eruption as obtained by an analogous method (Davydova et al., 2022). The products referred to are cristobalite- and tridymite-bearing rocks that were formed during the eruption of magma stored in the conduit under a lava plug (Davydova et al., 2022), hence were the first portions of magma that were discharged to the ground surface during the December 20, 2017 eruption. Comparison of bulk rock and mineralogical composition of the lapilli with the products of the December 2017 eruption referred to above has enabled us to trace changes in the volcano's magma plumbing system.

The composition of the eruptive products. The volcanic products discharged by the April 2017 eruption are basaltic andesites whose compositions roughly follow the evolutionary trend for the compositions of rocks discharged during the current eruptive cycle as pointed out previously (Malyshev, 2000; Turner et al., 2013). However, the rocks sampled from juvenile blocks in the pyroclastic flow have practically identical bulk rock compositions, and plot in the region of the compositions of highest basicity discharged by Bezymianny, while the lapilli show a broader compositional range (55.5–57 wt % SiO_2). Similar variations in chemical composition are also noted for some other eruptions (e.g., October 14–15, 2007 or December 20, 2017, see Fig. 3).

It has been shown for the December 20, 2017 eruption that this broad compositional range is due to the output of evolved magma that was formed in the upper part of the magma chamber, or even at the top of the magma conduit during the relatively long repose period of this volcano in 2012–2016, while the bulk of the material that reflected the magma composition in the shallow chamber and which composes the pyroclastic flows is comparatively homogeneous as to chemical composition and corresponds with the most primitive part of the range (Davydova et al., 2022). Such relatively felsic varieties of eruptive products were noted for all studied eruptions that have occurred after the intermission until 2020 (2016–2020) (Mania et al., 2019; Koulakov et al., 2021; Davydova et al., 2022, unpublished data).

The pyroclastic flows that are due to the eruptions of 2022 and 2023 do not contain such comparatively felsic material, according to our field observations. The earlier magma portions that were erupted on April 7, 2023 as tephra—pumice lapilli—do not show any significant displacement to the high silica region, although demonstrating some compositional diversity. The above argument suggests that the series of the successive 2017–2020 eruptions have effectively removed from the top of the magma chamber most of the magma that had been evolving during the repose period (2012–2016). At present the magma plumbing system has returned to a state that is analogous to that before 2012 with a relatively homogeneous shallow magma chamber whose magma is consistent with basaltic andesites by its chemical composition.

The increasing mean values of thermal power for the volcano (see Fig. 7) and the fact that the distribution of the plots showing thermal emission power has returned to that observed during the period 2000–2012 (Fig. 8), also constitute indirect evidence that the magma plumbing system has passed through the "transitional period" due to the intermission of explosive activity.

Variations in copper concentration in eruptive products. It was previously been pointed out for the rocks discharged during the current eruption cycle of Bezymianny Volcano that mafic enclaves were anomalously enriched in copper (150–330 ppm) in contrast to the host andesites and basaltic andesites, which contain relatively low (30–50 ppm) Cu concentrations for rocks of this composition (Davydova et al., 2017;

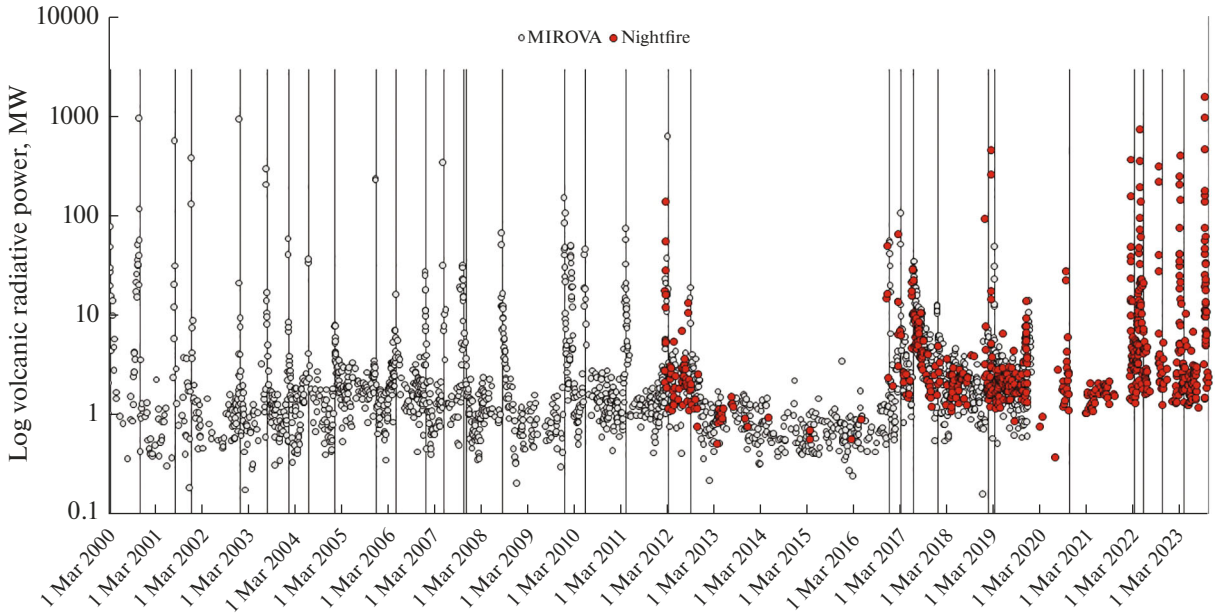

Fig. 8. The plot of thermal emission distribution on Bezymianny Volcano for the period 2012–2023 based on data of VIIRS Nightfire satellite monitoring compared with previously published data acquired using the MIROVA algorithm (Coppola et al., 2021) based on the distribution of thermal emission before the intermission of explosive activity during the period 2012–2016. Black vertical lines mark eruption dates.

Davydova et al., 2024). The basaltic andesites considered in this study are characterized by a higher concentration of copper (65–80 ppm) compared with the andesites and basaltic andesites discharged by the eruptions of the last two decades (30–50 ppm, see Fig. 4a, Davydova et al., 2024) and during the entire current eruption cycle (18–63 ppm, (Turner et al., 2013)). The lapilli are also characterized by higher concentrations of Cu (80 ppm) relative to bombs from the pyroclastic flow (65 ppm). On the contrary, mafic enclaves have a composition that plots in the region of least copper-rich compositions of mafic enclaves for Bezymianny Volcano (150 ppm for the 2023 enclaves and 100–330 ppm for the 2007–2017 enclaves, see Davydova et al., 2024) (see Fig. 4b). Previously we proposed a mechanism to explain the enrichment of Bezymianny basaltic andesites in Cu by appealing to the idea of its redistribution into mafic enclaves in the magma chamber (Davydova et al., 2024).

The relatively low enrichment of mafic enclaves in copper and persisting higher concentrations of copper in basaltic andesites may have occurred in a short time interval between the supply of magma from the lower levels of the system into the shallow chamber, and the eruption. The differences between the compositions of lapilli and bombs can be explained as resulting from their formation from magmas stored in different parts of the magma chamber, with lapilli which were among the first to be discharged being probably formed of the magma residing in the upper parts of the chamber or in the magma conduit itself, and experiencing a minimal interaction with the magma of the mafic enclaves. However, the observed differences can also provide evidence of considerable changes in the magmatic processes that led to eruptions of Bezymianny and controlled the behavior of copper in its magma plumbing system, and call for further study.

CONCLUSIONS

The volcanic products of the April 7, 2023 eruption are medium-K basaltic andesites. The compositions of rocks from juvenile bombs and blocks of pyroclastic flows plot in the region of the most primitive rocks discharged during the current eruption cycle. The lapilli show a broader compositional range; they were formed from the magma stored just before the eruption in the upper part of the magma chamber. The magma had temperatures reaching 980°C just before the eruption.

The environment of formation and the mineral composition of the rocks provide evidence of an effective removal from the upper part of the Bezymianny shallow magma chamber of the bulk of the magma that had been evolving toward greater acidity during the repose period of 2012–2016, thus showing that the shallow chamber had returned to the state that was the most similar to that during the period 2007–2012.

There is an interesting difference from the products of previous eruptions in that a higher concentration of copper in basaltic andesites compared with the previous eruptions was observed, but the nature of this phenomenon requires more detailed studies.

ABBREVIATIONS AND NOTATION

RAS	Russian Academy of Sciences
FEB	Far East Branch
IVS	Institute of Volcanology and Seismology
CSU IGEM RAS	Center of Shared Use, Institute of Geology of Ore Deposits, Petrography, Mineralogy, and Geochemistry, Russian Academy of Sciences

ACKNOWLEDGMENTS

We are grateful to colleagues in the *Eruptivnyi* team of the Institute of Volcanology and Seismology FEB RAS who took part in the field work in April 2023, including I.A. Nuzhdaev and V.I. Frolov who lent us photographic materials; S.Z. Smirnov and T.Yu. Timina who provided us with the compositions of volcanic ash; D.S. Tatarinova and M.D. Shchekleina for their help the field work in August 2023, and I. Abkadyrov for his help in transportation of the samples.

FUNDING

This work was supported by the Russian Science Foundation, project no. 22-77-00016.

CONFLICT OF INTEREST

The authors of this work declare that they have no conflicts of interest.

REFERENCES

Albarede, F., How deep do common basaltic magmas form and differentiate? *J. Geophys. Res.: Solid Earth,* 1992, vol. 97, no. B7, pp. 10997–11009.

Coppola, D., Laiolo, M., Massimetti, F., Hainzl, S., Shevchenko, A., Mania, R., Shapiro, N., and Walter, T.R., Thermal remote sensing reveals communication between volcanoes of the Klyuchevskoy Volcanic Group, *Scientific Reports,* 2021, vol. 11, no. 1, pp. 13 090.

Davydova, V.O., Shcherbakov, V.D., Plechov, P.Yu., and Perepelov, A.B., Petrology of mafic enclaves in the 2006–2012 eruptive products of Bezymianny volcano, Kamchatka, 2006–2012, *Petrologiya,* 2017, vol. 25, no. 6, pp. 592–614.

Davydova, V.O., Shcherbakov, V.D., and Plechov, P.Yu., The Timescales of Magma Mixing in the Plumbing System of Bezymianny Volcano (Kamchatka): Insights from Diffusion Chronometry. *Moscow University Geology Bulletin.,* 2018, no. 73(5), pp. 444–450.

Davydova, V.O., Shcherbakov, V.D., Plechov, P.Y., and Koulakov, I.Y., Petrological evidence of rapid evolution of the magma plumbing system of Bezymianny volcano in Kamchatka before the December 20th, 2017 eruption, *J. Volcanol. Geotherm. Res.,* 2022, vol. 421, pp. 107–422.

Davydova, V.O., Shcherbakov, V.D., Plechov, P.Y., Yapaskurt, V.O., Scherbakov, Yu.D., Perepelov, A.B., Brianskii, N.V., and Antipin, V.S., Copper redistribution from shallow oxidized magmas to mafic enclaves. Insight from anomalously Cu-enriched enclaves from Bezymianny volcano, Kamchatka, *Lithos,* 2024. https://doi.org/10.2139/ssrn.4661224

Elvidge, C., Zhizhin, M., Hsu, F-C., and Baugh, K., VIIRS Nightfire: Satellite pyrometry at night, *Remote Sensing*, 2013, vol. 5, no. 9, pp. 4423–4449.

Girina, O.A., Chronology of Bezymianny volcano activity, 1956–2010, *J. Volcanol. Geotherm. Res.,* 2013, vol. 263, pp. 22–41.

Girina, O.A., Gorbach, N.V., Davydova, V.O., Melnikov, D.V., Manevich, T.M., Manevich, A.G., and Demyanchuk, Yu.V., The 15 March 2019 Bezymianny Volcano explosive eruption and its products, *J. Volcanol. Seismol.,* 2020, vol. 14, no. 6, pp. 394–409.

Girina, O.A., Loupian, E.A., Manevich, A.G., Melnikov, D.V., Nuzhdaev, A.A., Sorokin, A.A., Romanova, I.M., Kramareva, L.S., Uvarov, I.A., Korolev, S.P., Demyanchuk, Yu.V., and Tsvetkov, V.A., Remote monitoring of explosive eruptions on Bezymianny Volcano in 2023, in *Materialy 21-i Mezhdunarodnoi konferentsii "Sovremennye problemy distantsionnogo zondirovaniya Zemli iz kosmosa"* (Proc. 21st Intern. Conf. "Modern Problems in Remote Sounding of Earth from Space"), XXI.G.92, Moscow, November 13–17, 2023, Moscow: IKI RAN, 2023.

Jarosewich, E., Nelen, J.A., and Norberg, J.A., Reference samples for electron microprobe analysis, *Geostandards Newsletter,* 1980, vol. 4, no. 1, pp. 43–47.

Koulakov, I., Plechov, P., Mania, R., Walter, T.R., Smirnov, S.Z., Abkadyrov, I., Jakovlev, A., Davydova, V., Senyukov, S., Bushenkova, N., Novgorodova, A., Stupina, T., and Droznina, S.Ya., Anatomy of the Bezymianny volcano merely before an explosive eruption on 20.12.2017, *Scientific reports,* 2021, vol. 11, no. 1, pp. 1–12.

Malyshev, A.I., *Zhizn vulkana* (The Life of Volcanoes), Yekaterinburg: UrO RAN, 2000.

Melnikov, D.V., Zhizhin, M.N., Trifonov, G.M., and Poida, A.A., The dynamics of the 2012–2017 eruption of Snow Volcano (Chirpoi Island, Kuriles): Results from an application of the VIIRS Nightfire algorithm, *Sovr. Probl. Dist. Zond. Zemli iz Kosmosa,* 2018, vol. 15, no. 3, pp. 69–79.

Mueller, S., Scheu, B., Kueppers, U., Spieler, Richard D., and Dingwell, D., The porosity of pyroclasts as an indicator of volcanic explosivity, *J. Volcanol. Geotherm. Res.,* 2011, vol. 203, pp. 168–174.

Plechov, P., Blundy, J., Nekrylov, N., Melekhova, E., Shcherbakov, V., and Tikhonova, M.S., Petrology and volatile content of magmas erupted from Tolbachik Volcano, Kamchatka, 2012–2013, *J. Volcanol. Geotherm. Res.,* 2015, vol. 307, pp. 182–199.

Putirka, K.D., Thermometers and barometers for volcanic systems, *Rev. Mineral. Geochem.,* 2008, vol. 69, no. 1, pp. 61–120.

Shcherbakov, V.D., Plechov, P.Y., Izbekov, P.E., and Shipman, J.S., Plagioclase zoning as an indicator of magma processes at Bezymianny Volcano, Kamchatka, *Contrib. Mineral. Petrol.,* 2011, vol. 162, pp. 83–99.

Senyukov, S.L., Nuzhdina, I.N., Droznina, S.Ya., Kozhevnikova, T.Yu., Nazarova, Z.A., and

Sobolevskaya, O.V., The 2022–2023 seismicity of Bezymianny Volcano, in *Trudy Devyatoi Vserossiiskoi nauchn-tekhnicheskoi konferentsii s mezhdunarodnym uchastiem* (Proc. 9th Science Conference with International Participation), September 24–30, 2023, *"Problemy kompleksnogo geofizicheskogo monitoringa seismoaktivnykh regionov"* (Problems in the Multidisciplinary Geophysical Monitoring of Seismic Regions), Petropavlovsk-Kamchatsky, 2023, pp. 183–187.

Trifonov, G., Zhizhin, M., Melnikov, D., and Poyda, A., VIIRS Nightfire remote sensing volcanoes, *Procedia Computer Science,* 2017, vol. 119, pp. 307–314.

Turner, S.J., Izbekov, P.E., and Langmuir, C., The magma plumbing system of Bezymianny Volcano: Insights from a 54 year time series of trace element whole-rock geochemistry and amphibole compositions, *J. Volcanol. Geothermal. Res.,* 2013, vol. 263, pp. 108–121.

Zhizhin, M., Matveev, A., Ghosh, T., Hsu, F-C., Howells, M., and Elvidge, C., Measuring gas flaring in Russia with multispectral VIIRS Nightfire, *Remote Sensing*, 2021, vol. 13, no. 16, pp. 3078.

Translated by A. Petrosyan